DEVELOPMENT OF MINI VIBRATION-POWERED GENERATOR

[1]WEN-DIAN LOU, [2]SHENG-CHING WANG, [3]YU-CHI WU, [4]JIN-YUAN LIN

[1,2]Department of Mechanical Engineering, National United University, Taiwan 360, R.O.C.
[3,4]Department of Electrical Engineering, National United University, Taiwan 360, R.O.C.
E-mail: [1]x711058@gmail.com, [2]lywang@nuu.edu.tw, [3]ycwu@nuu.edu.tw, [4]yuan@nuu.edu.tw

Abstract- This study aims to design a mini vibration-powered generator to acquire the vibration power in the nature. With the electromagnetic field simulation software, ANSYS Maxwell, and the circuit analysis software, ANSYS Simplorer, we evaluate the generator performance by converting its alternating voltage to stable direct voltage for a resistive load. Then the generator performance is evaluated with the load voltage. Furthermore, Taguchi method is utilized for analyzing the optimal combination of permanent magnet size and core diameter size for the generator. Finally, a vibration-powered generator based on the proposed design is realized, and its property is actually measured.

Keywords- Vibration-powered generator, ANSYS Maxwell, ANSYS Simplorer, Taguchi Method.

I. INTRODUCTION

The major power generation in the world currently relies on thermal power generation, which converts thermal energy to electric energy by burning fossil fuels but results in air pollution [1]. To reduce the pollution caused by power generation, distinct green alternative energy has been gradually developed, such as wind power generation and solar power generation. However, the installation of such alternative energy costs a lot.

Except for solar energy and wind energy, thermal energy and vibration energy [2] are two feasible options and often appear in the energy harvesting process. Vibration energy would be generated by mechanical operation and is ubiquitous in the living environment. When such unused vibration energy is collected, the benefits would be considerable. This study therefore aims to develop a rod-shaped mini vibration-powered generator [3] to collect vibration energy, expecting that many a little makes a mickle.

II. ROD-SHAPED MINI VIBRATION-POWERED GENERATOR MODEL

Fig. 1 shows the structure of a rod-shaped vibration-powered generator. The mini generator is combined with permanent magnets and coil. In order to reduce the simulation and analysis time, the model is simplified from 3D to 2D model, shown in Fig. 2, where Dc is the coil outside diameter, Dm is the permanent magnet outside diameter, Dmi is the permanent magnet inside diameter, w is the coil thickness, δ is the gap between coil and permanent magnets, l is the air gap between two permanent magnets, hm is the permanent magnet height, and hc is the coil height.

In the model, the quantity of permanent magnets used and their arrangement would affect the back electromotive force of coil induction. Under the same quantity of the permanent magnets used, the permanent magnet arrangement could be divided into Halbach array type (1st type), Magnetic repulsion type (2nd type), and Magnetic pole in same direction type (3rd type)[4], shown in Fig, 3. The 1st type, Halbach array type, is arranged with magnets in radial and axial directions. Similar to the magnetic circuit direction of the 2nd type (Magnetic repulsion type), Halbach array type aims to focus on the flux linking coil to increase the induced voltage. For selecting a better vibration-powered generator structure, the electromagnetic field software ANSYS Maxwell is further applied to analyze these three types and compare their differences.

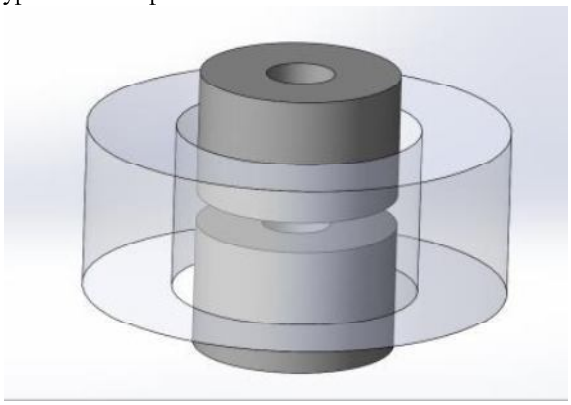


Fig. 1 Rod-shaped vibration-powered generator model

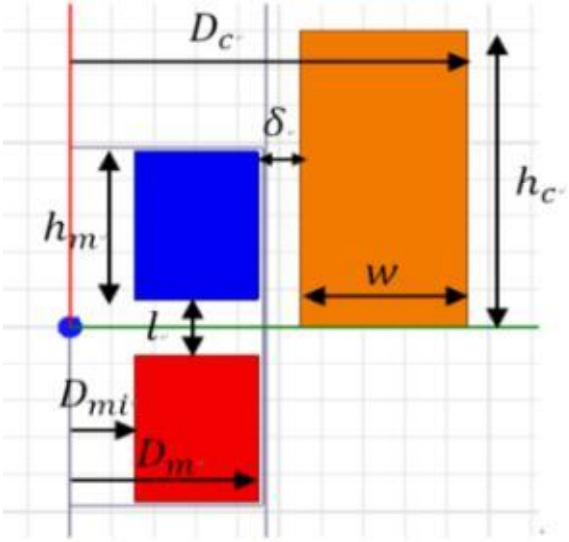


Fig. 2 2D model and parameters

III. MAXWELL ELECTROMAGNETIC FIED SIMULATION ANALYSIS

According to Farady's law of induction, the electromotive force ε generated in a coil is proportional to the rate of change of magnetic flux going through the coil plane, as the following equation.

$$\varepsilon = -\frac{d\emptyset}{dt} \qquad (3.1)$$

where ε is the induced electromotive force, $d\emptyset$ is the amount of change of magnetic flux $\emptyset$ within the time dt, and the minus sign denotes the direction of induced electromotive force. When the coil has total N turns and the rate of change of magnetic flux in each turn is the same, the sum of electromotive force is

$$\varepsilon = -\mathrm{N}\frac{d\emptyset}{dt} \qquad (3.2)$$

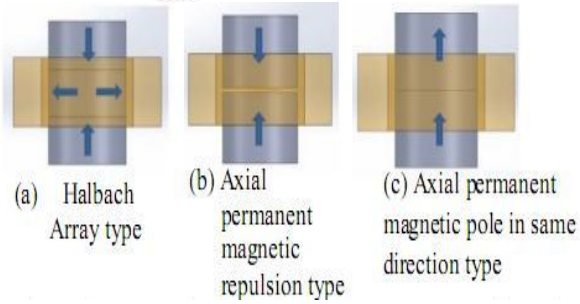


Fig. 3 Three types of permanent magnet arrangement of the rod- shaped vibration-powered generator

Since the magnetic flux $\emptyset = BA$ passing through the coil, where B is the air gap magnetic flux density (in unit Tesla) and A is the area (in unit $m2$) that the magnetic flux passes through, the equation of induced electromotive force is further presented as

$$\varepsilon = -\mathrm{N}\frac{d(BA)}{dt} = -NBlv \qquad (3.3)$$

where l is the effective length that the magnetic flux passes through and v is the coil moving speed. The induced electromotive force therefore is proportional to the number of turns, air gap magnetic flux density, speed, and effective length.

As mentioned in previous section, the arrangement and the polarity of permanent magnets in the vibration-powered generator would affect the induction voltage. In order to compare the difference among these three different types shown in Fig. 3, merely the arrangement of permanent magnets is changed in the Maxwell 2D simulation (hm is 2.8mm for the 1st type and 4mm for both 2nd and 3rd types), while other parameters are unchanged (hc=8mm, w=4mm, Dc=17mm, N=2087 turns, Dm=7mm, Dmi=3.1mm, vibration frequency=30Hz, vibration stroke=8mm).

When simulating the generator transient with Maxwell 2D, an observation line is pre-drawn on the coil average circumference for observing the air gap magnetic flux density distribution. The line of magnetic force distribution in the 1st type is similar to that in the 2nd type. The line of magnetic force distribution in the 3rd type focuses on both ends of the permanent magnet and is axially divergent, while the magnetic force distribution in the 1st type and the 2nd type concentrates on the radial permanent magnet position, shown in Fig. 4, where the magnetization direction of permanent magnet is shown with an arrow.

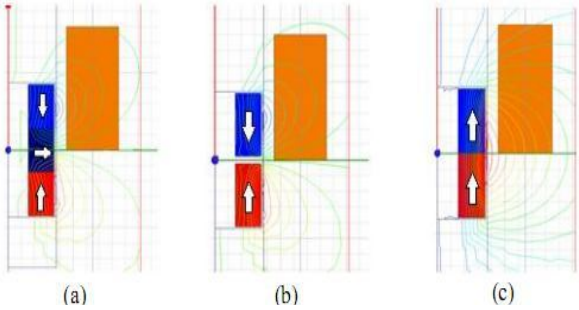
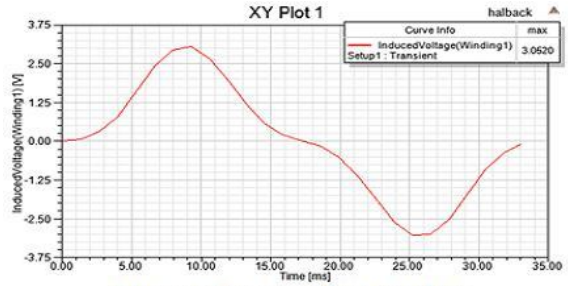


Fig. 4 (a) Halback array type, (b) Magnetic repulsion type, (c) Magnetic pole in same direction type

Based on the pre-drawn observation line, the air gap magnetic flux density distribution in three types of generators can be acquired. The air gap magnetic flux density and the back electromotive force of the 1st type, shown in Fig. 5, are higher than those of other two types shown in Figs. 6 and 7. The air gap magnetic flux density distribution in the 2nd type is similar to that in 1st type, and the back electromotive force value is also close to that in the 1st type, shown in Fig. 6. Under the same simulation conditions, the air gap magnetic flux density and the back electromotive force value of Magnetic pole in the 3rd type are lower than those of other two types, but the back electromotive force waveform approaches sinusoidal wave, shown in Fig. 7. As a result, the permanent magnet arrangement of the 2nd type is utilized for the design of the mini vibration-powered generator for its easy implementation.



(a) Air-gap magnetic flux density distribution

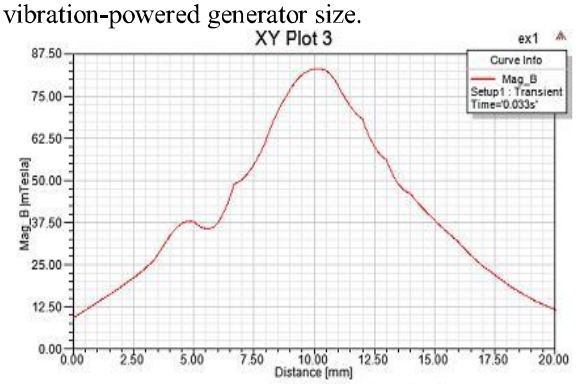


(b) Back electromotive force waveform

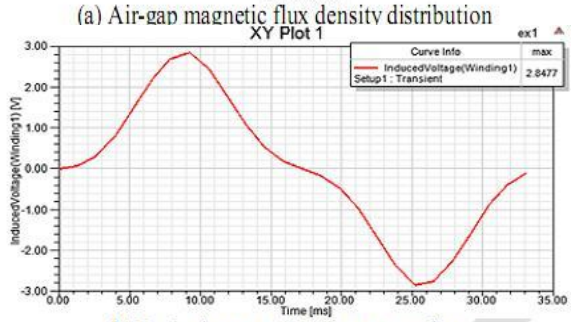
Fig. 5 Halback array type

IV. SIMPLORER CIRCUIT SIMULATION ANALYSIS

The induced voltage generated by the mini vibration-powered generator in the Maxwell electromagnetic field simulation is open-circuit voltage, and the internal resistance of the generator and load are not taken into account. To make sure that the generated electric power can stably provide the load and to analyze its effect, the Simplorer circuit simulation software is further used for modifying the mini vibration-powered generator size.

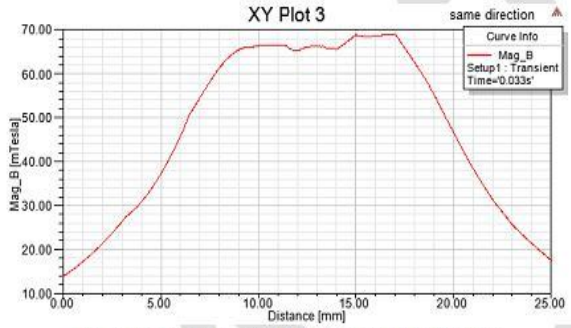


(a) Air-gap magnetic flux density distribution

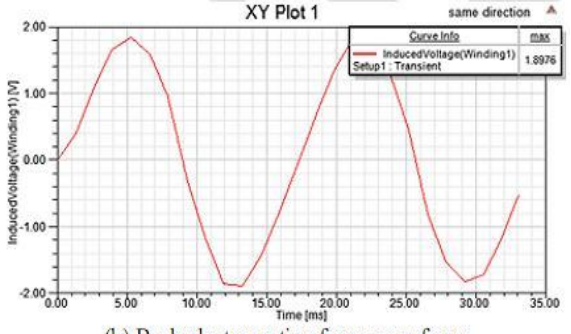


(b) Back electromotive force waveform

Figure 6 Magnetic repulsion type



(a) Air-gap magnetic flux density distribution



(b) Back electromotive force waveform

Fig. 7 Magnetic pole in same direction type

In the Maxwell 2D simulation, the back electromotive force waveform of the 2nd type approaches sinusoidal wave so that the alternating voltage source is used to replace the mini vibration-powered generator in the circuit simulation, shown in Fig. 8.

In Fig. 8, the internal resistance R1 would change with the mini vibration-powered generator size, the bias voltage of the bridge rectifier is 0.7V, the load resistance R5=100Ω, and the filter capacitor C1=0.001F, shown in Table 1. The alternating voltage waveform of the simulated vibration-powered generator can be measured by the voltmeter of the simulation circuit; the frequency is 30Hz, shown in Fig. 9, and the load voltage after the rectification is around 2.64V, shown in Fig. 10.

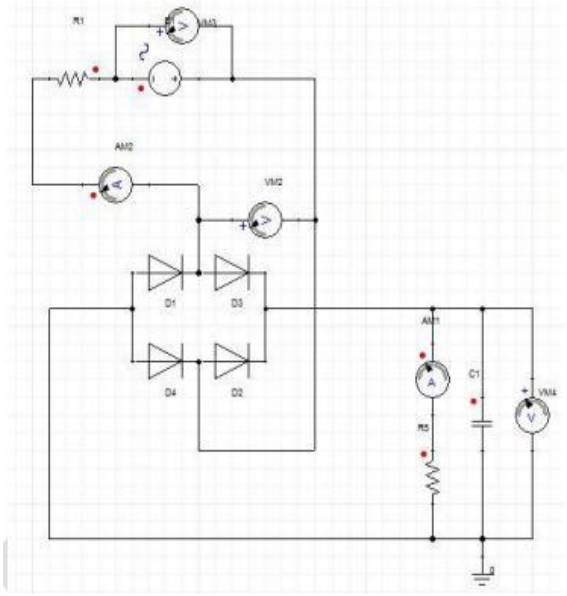


Figure 8 Simplorer simulation circuit

Table 1: Circuit Element Parameter

Internal resistance R1 of mini vibration-powered generator	57.6Ω
Load resistance R5	100Ω
Bridge rectification diode bias voltage	0.35V
Filter capacitor C1	0.001farad
Internal resistance R1 of mini vibration-powered generator	57.6Ω
Load resistance R5	100Ω
Bridge rectification diode bias voltage	0.35V
Filter capacitor C1	0.001F

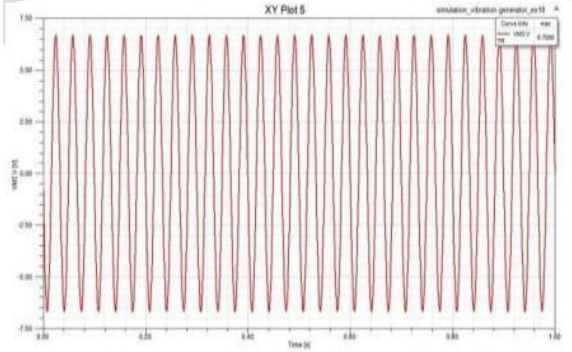


Fig. 9 Measured alternating voltage waveform of voltage source

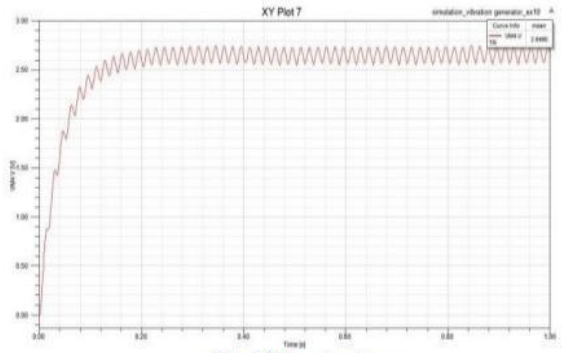


Fig. 10 Load voltage

V. TAGUCHI METHOD ANALYSIS

To search for the proper vibration-powered generator size, Taguchi Method [5] is utilized in this study for rapidly finding out the best parameter combination. In the vibration-powered generator, the factors affecting the power generation voltage are permanent magnet outside diameter *Dm*, permanent magnet thickness *hm*, copper core diameter, and space l between two permanent magnets. Three levels of specifications are selected, shown in Table 2. An orthogonal table could list all possible combinations as well as reduce the number of experiments.

Table 2:3-level 4-factor table

Factor		Level 1	Level 2	Level 3
A	copper core diameter	0.1 mm	0.15 mm	0.2 mm
B	l	0.5 mm	1 mm	1.5 mm
C	D_m	7 mm	9 mm	11 mm
D	h_m	4 mm	6 mm	8 mm

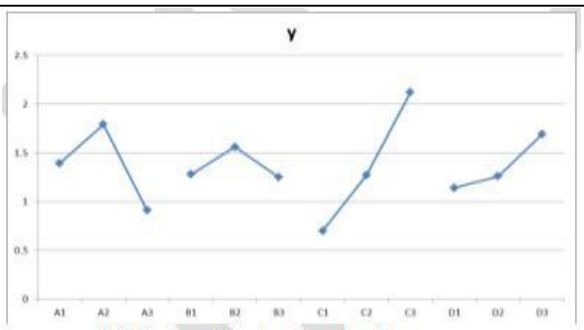
With the electromagnetic field simulation, the terminal voltage of the 9 combinations is listed in Table 3, where y is the load voltage and S/N is the signal-noise ratio of load voltage. Since the better generator property appears on the larger load voltage that larger-the-better equation (5.1) is used to determine the best design.

$$\frac{S}{N} = -\log\frac{1}{y^2} \qquad (5.1)$$

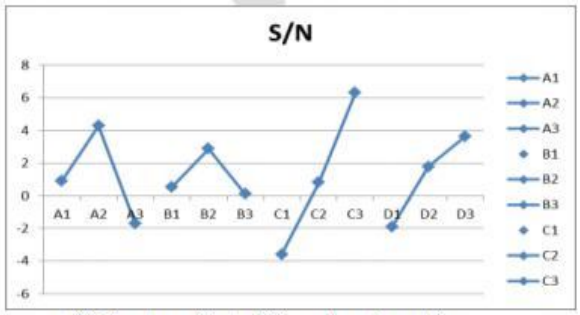
The experimental results are made for the factor effect table and further drawn the factor effect diagram, shown in Fig. 11.

Table 3 L9 Orthogonal Table and Experimental Data-factor effect

L9	A	B	C	D	y	S/N
1	1	1	1	1	0.42	-7.53501
2	1	2	2	2	1.39	2.860296
3	1	3	3	3	2.36	7.45824
4	2	1	2	3	1.94	5.756035
5	2	2	3	1	2.52	8.028011
6	2	3	1	2	0.9	-0.91515
7	3	1	3	2	1.48	3.405234
8	3	2	1	3	0.77	-2.27019
9	3	3	2	1	0.49	-6.19608



(a) Factor effect on load voltage



(b) Factor effect of signal-noise ratio

Fig. 11 Factor effect diagram

From the factor effect table, the optimal combination shows A2, B2, C3, and D1. The simulation software is further applied to re-simulate the load voltage of the optimal combination, which achieves 2.71V. In comparison with the initially designed generator and the one with the optimal combination, the load voltage of the latter appears 0.19V higher. A higher and stable voltage could be acquired when increasing the load resistance to reduce the discharging speed of the capacitor, shown in Fig. 12.

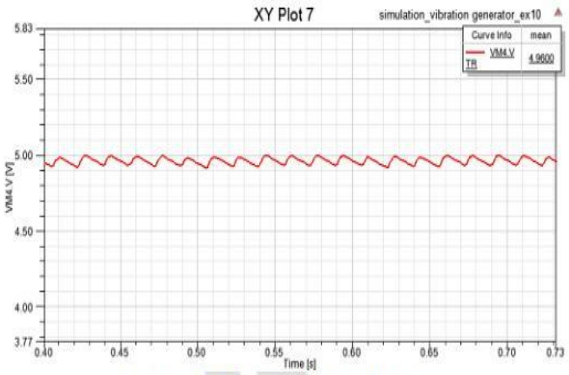


Figure 12 More stable load voltage

VI. MOTION SYSTEM WITH DAMPING CHARACTERISTICS

In consideration of damping existing in a spring and mass system, the permanent magnet vibrator of the vibration-powered generator would not maintain constant vibration. In a spring and mass system, the coefficient of damping C could be calculated with the differential equation of motion (5.2), and the fixed frequency Wn and the damping ratio ζ are further calculated with equations (5.3) and (5.4).

$$m\ddot{x} + c\dot{x} + kx = 0 \quad (5.2)$$

$$w_n = \sqrt{\frac{k}{m}} \quad (5.3)$$

$$\zeta = \frac{c}{2\sqrt{km}} \quad (5.4)$$

After the calculation, the system in this study is an underdamped system expressed as the equation of motion (5.5), where wd is the vibration frequency under the underdamped state and can be expressed as Eq. (5.6).

$$x(t) = Ae^{-\zeta w_n t}\cos(w_d + \varphi) \quad (5.5)$$

$$w_d = w_n\sqrt{1-\zeta^2} \quad (5.6)$$

Taking the underdamping characteristics into account, the amplitude of spring of the vibration-powered generator in the simulation reveals decline, shown in Fig. 13. The speed of the permanent magnetic field linking the coil decreases with declining vibration amplitude so that the back electromotive force waveform gradually declines, shown in Fig. 14.

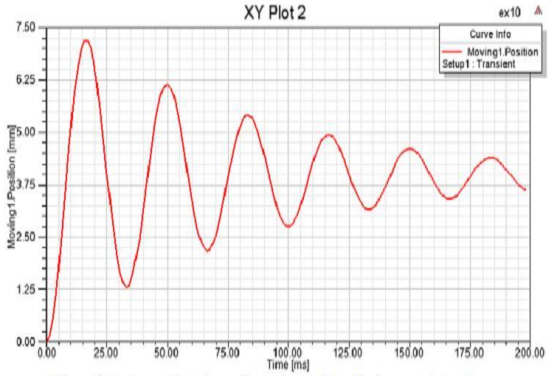


Fig. 13 Amplitude of spring declining with time

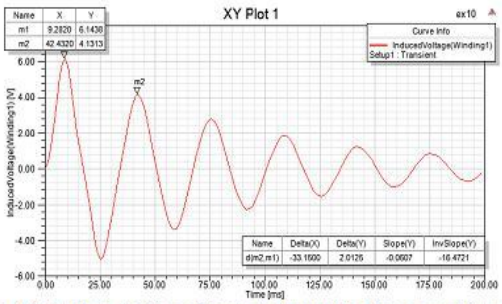


Fig. 14 Gradual decline of back electromotive force waveform of the generator

VII. REALIZATION OF ROD-SHAPED VIBRATION-POWERED GENERATOR

The 3D model with the best combination selected with Taguchi Method to design the overall structure of the generator is shown in Fig. 15. The generator body is composed of coil and two magnetically repulsive magnets. For the linear motion of magnets, linear bearing, roller, and spring are used for this design, and the permanent magnet is fixed on the roller and covered with a spring. The internal spring would store and release energy because of the external force so that the permanent magnet vibrates in the coil, where the vibration frequency relies on the natural frequency of the spring.

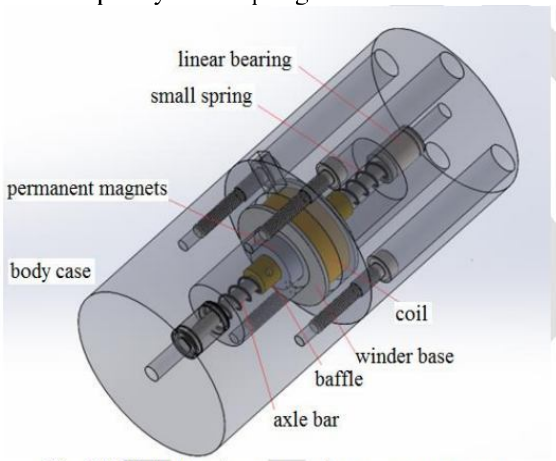


Fig. 15 Mini vibration-powered generator structure

The realized vibration-powered generator is shown in Fig. 16, covering the permanent magnet structure in the middle, the springs on both ends of the permanent magnet stopper, and the coil on the winder base. The real-size parameters of the vibration-powered generator are listed in Table 4.

VIII. REALIZATION OF ROD-SHAPED VIBRATION-POWERED GENERATOR

As previously mentioned, the voltage of the vibration-powered generator is an open-loop alternating signal that the rectifier circuit is required for rectifying the negative voltage into positive. Proper filter capacitors are further selected to stabilize the charging voltage for the load. Fig. 17 shows the rectifier circuit of the rod-shaped vibration-powered generator. In consideration of the voltage stability, two 220μF parallel capacitors are used for increasing the capacity and connected with a 2KΩ resistor to extend the discharge time. The circuit element parameters are listed in Table 5.

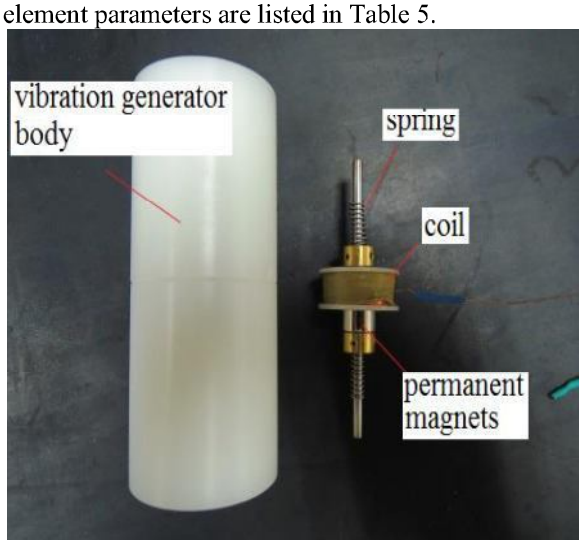


Fig. 16 Solid model of rod-shaped vibration-powered generator

Table 4:Rod-shaped Vibration-Powered GeneratorSize Parameter

Mini vibration-powered generator specification	Permanent magnetic repulsion type
Coil height (h_c)	8mm
Coil thickness (w)	4mm
Coil outside diameter (D_c)	21mm
Coil number of turns (N)	1040 turn
Permanent magnet height (h_m)	8mm
Permanent magnet outside diameter (D_m)	11mm
Permanent magnet inside diameter (D_{mi})	3.1mm
Air gap (δ)	1.2mm
Vibration stroke	8mm
Total generator length	90mm
Generator outside diameter	40mm

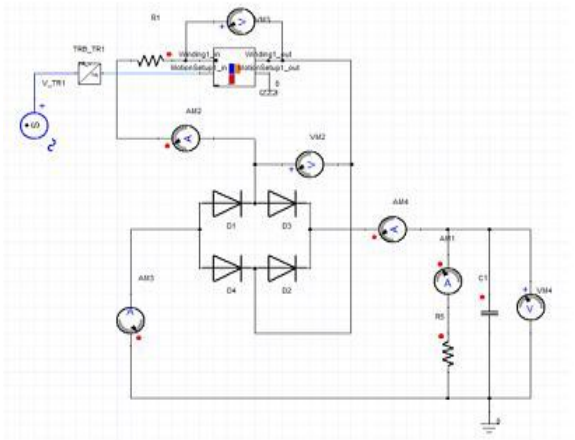


Fig. 17 Rectification circuit of the vibration-powered generator

Table 5: Circuit Element Parameter

Generator internal resistance	55.6Ω
Commutator bias voltage	1V
Filter capacitor	$220\mu f$*2
Load resistance	2KΩ

By knocking the vibration-powered generator body, the internal permanent magnet vibrates with the natural frequency of spring. From the observation through an oscilloscope, the open-loop back electromotive force of the generator could reach up to 6V, with the vibration frequency about 30Hz, while the voltage amplitude gradually declines with the consumption of spring damping, shown in Fig. 18. When the voltage passes through the rectifier, the voltage frequency grows twice and the amplitude is slightly lower by 1V. The voltage after the rectification provides power to the load after the capacitor filter. From Fig. 19, the capacitor provides 2V stable voltage for 2KΩ load. Furthermore, the equation P=V×I reveals that the generator provides 2mW power to the load. By replacing 2KΩ current-limiting resistor with an LED connected with an 820Ω resistor, we can further obtain the capacitor discharging curve shown in Fig. 20. The discharge speed of the capacitor is faster than that in the pure load circuit, but it allows the LED stably and continuously illuminating, shown in Fig. 21.

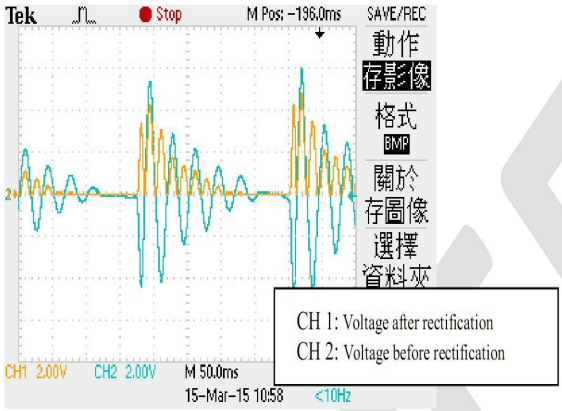


Fig. 18 Waveform comparison before and after rectification

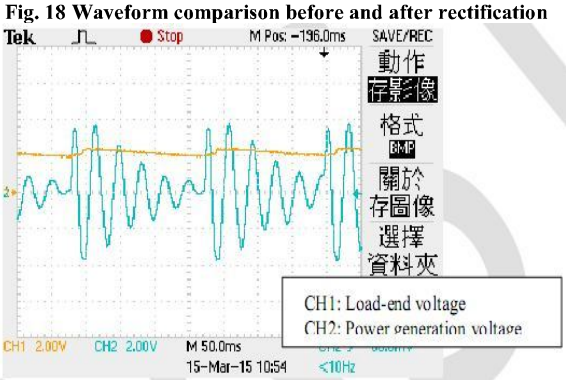


Fig. 19 Comparison between generator voltage and load voltage when load is a pure resistor 2KΩ

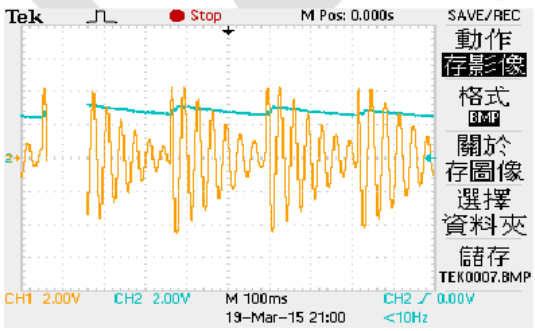


Fig. 20 Comparison between generator voltage and load voltage when the load is an LED with a resistor 820Ω

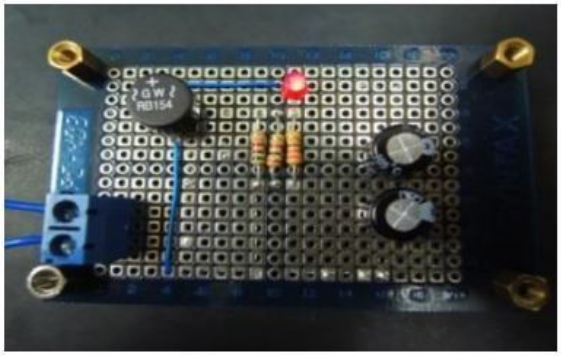


Fig. 21 Generator stably supplying power for LED

CONCLUSIONS

In this study, the internal permanent magnet structure of the mini vibration-powered generator is initially assumed to vibrate with stable vibration sources. The Simplorer circuit simulation reveals that higher load voltage and generation power could be acquired with stable vibration sources. Therefore, the load voltage could be used as the larger-the-better indicator in Taguchi Method for selecting the optimal combination.

In consideration of the actual power generation, the underdamping caused by springs is added in the electromagnetic field simulation to understand the decline of the back electromotive force generated from the generator. The generation power of the vibration-powered generator is eventually measured in the experiment.

Although the measured power from the mini vibration-powered generator is merely 2mW, the selection of proper load resistance and filter capacitors allows the constant illumination of LED. When the entire system body is minimized and a group of the designed vibration generators are connected in series, they could provide power for higher load, or store the electric energy in batteries.

ACKNOWLEDGMENTS

We are grateful for the financial support from the Department of Engineering and Technologies, Ministry of Science and Technology, under the program 103-2815-C-239-015-E.

REFERENCES

[1]. T.W. Chuang, "Design and Experiments of Linear Permanent-Magnet Generator," Mater Thesis, Department of Mechanical Engineering, Kun Shan University, 2011.

[2]. C.C. Lin, "Manufacturing of a Vibrational Sheet Generator for Energy Harvesting," Mater Thesis, Graduate Institute of Lean Production Management, Hsiuping University of Science and Technology, 2011.

[3]. C.H. Chang, H.C. Tseng, and Y.W. Lin, "Fabrication of Energy-Saving Movable Charger," Journal of Kun Shan University of Technology, vol. 9, June 2012.

[4]. W.T. Lai, "A Study of Simple Thermal Energy Conversion Device," Mater Thesis, Department of Mechanical and Electro-Mechanical Engineering, National Sun Yat-Sen University, 2009.

[5]. H.H. Li, "Taguchi Methods: Principles and Practices of Quality Design," Department of Engineering Science, National Cheng Kung university. Gau Lih Book Co., Ltd.

★★★